AGU PUBLICATIONS

JGR

Journal of Geophysical Research: Space Physics

RESEARCH ARTICLE
10.1002/2015JA022321

Key Points:
- CEDDs obtained from pB measurements are similar to those from DH type II based on CME-streamer interactions
- 1-fold Saito's model is a proper CEDD for analyzing DH type II bursts
- CME shock-streamer interactions could be a plausible origin for generating DH type II bursts

Correspondence to:
Y.-J. Moon,
moonyj@khu.ac.kr

Citation:
Lee, J.-O., Y.-J. Moon, J.-Y. Lee, K.-S. Lee, and R.-S. Kim (2016), Coronal electron density distributions estimated from CMEs, DH type II radio bursts, and polarized brightness measurements, *J. Geophys. Res. Space Physics*, *121*, 2853–2865, doi:10.1002/2015JA022321.

Received 29 DEC 2015
Accepted 1 APR 2016
Accepted article online 5 APR 2016
Published online 25 APR 2016

Coronal electron density distributions estimated from CMEs, DH type II radio bursts, and polarized brightness measurements

Jae-Ok Lee[1], Y.-J. Moon[1,2], Jin-Yi Lee[2], Kyoung-Sun Lee[3], and R.-S. Kim[4]

[1]School of Space Research, Kyung Hee University, Yongin, South Korea, [2]Department of Astronomy and Space Science, Kyung Hee University, Yongin, South Korea, [3]Hinode Science Center, National Astronomical Observatory of Japan, Tokyo, Japan, [4]Korea Astronomy and Space Science Institute, Daejeon, South Korea

Abstract We determine coronal electron density distributions (CEDDs) by analyzing decahectometric (DH) type II observations under two assumptions. DH type II bursts are generated by either (1) shocks at the leading edges of coronal mass ejections (CMEs) or (2) CME shock-streamer interactions. Among 399 Wind/WAVES type II bursts (from 1997 to 2012) associated with SOHO/LASCO (Large Angle Spectroscopic COronagraph) CMEs, we select 11 limb events whose fundamental and second harmonic emission lanes are well identified. We determine the lowest frequencies of fundamental emission lanes and the heights of leading edges of their associated CMEs. We also determine the heights of CME shock-streamer interaction regions. The CEDDs are estimated by minimizing the root-mean-square error between the heights from the CME leading edges (or CME shock-streamer interaction regions) and DH type II bursts. We also estimate CEDDs of seven events using polarized brightness (pB) measurements. We find the following results. Under the first assumption, the average of estimated CEDDs from 3 to 20 R_s is about 5-fold Saito's model ($N_{\mathrm{Saito}}(r)$). Under the second assumption, the average of estimated CEDDs from 3 to 10 R_s is 1.5-fold $N_{\mathrm{Saito}}(r)$. While the CEDDs obtained from pB measurements are significantly smaller than those based on the first assumption and CME flank regions without streamers, they are well consistent with those on the second assumption. Our results show that not only about 1-fold $N_{\mathrm{Saito}}(r)$ is a proper CEDD for analyzing DH type II bursts but also CME shock-streamer interactions could be a plausible origin for generating DH type II bursts.

1. Introduction

The coronal electron density is a fundamental and important physical quantity in solar physics. Several methods for determining the coronal electron density have been proposed as follows (*Leblanc et al.* [1998], *Aschwanden* [2005], and *Wang and Davila* [2014] for reviews). First, using white light observations, coronal electron density distributions (CEDDs) have been derived from polarized brightness (pB) measurements. Early researchers used the data of solar eclipses detected by ground-based white light K-coronameters to determine CEDDs from about 1 to 3 solar radius (R_s) [*van de Hulst*, 1950; *Newkirk*, 1961; *Saito*, 1970]. The white light coronagraph data of satellites (Large Angle Spectroscopic COronagraph (LASCO); *Brueckner et al.*, 1995, on board the Solar and Heliospheric Observatory (SOHO) and coronagraphs of Sun Earth Connection Coronal and Heliospheric Investigation (SECCHI); *Howard et al.*, 2008, on board the Solar TErrestrial Relations Observatory (STEREO)) have been used to estimate CEDDs from about 1.5 to 6 R_s or up to 30 R_s [*Saito et al.*, 1977; *Hayes et al.*, 2001; *Gopalswamy and Yahiro*, 2011; *Wang and Davila*, 2014]. Second, using ultraviolet (UV) spectral observations, the ratio of radiative and collisional components of the O VI doublet in spectra has been used for the determination of coronal densities from about 1.5 to 5 R_s [*Noci et al.*, 1987; *Parenti et al.*, 2000; *Ko et al.*, 2006; *Uzzo et al.*, 2006; *Lee et al.*, 2008]. Several density sensitive lines also can be used with the CHIANTI atomic database to derive coronal densities from about 1.1 to 3.5 R_s [*Keenan et al.*, 1995; *Pinfield et al.*, 1998; *Gibson et al.*, 1999; *Akmal et al.*, 2001; *Lee et al.*, 2009]. Third, using radio observations, CEDDs from about 2 to 215 R_s have been determined by analyzing type III radio bursts [*Fainberg and Stone*, 1971; *Alvarez and Haddock*, 1973; *Leblanc et al.*, 1998]. Several researchers have investigated CEDDs from about 3 to 30 R_s using type II radio bursts and coronal mass ejections (CMEs) [*Robinson and Stewart*, 1985; *Reiner et al.*, 2003; *Pohjolainen et al.*, 2007].

The CME-driven shocks can cause type II radio bursts through the following physical processes: (1) a CME-driven shock accelerates nonthermal electrons, (2) the accelerated electrons produce Langmuir waves in the surrounding areas of the shock, and (3) the Langmuir waves are converted into radio emissions at the fundamental and second harmonic of the local plasma frequency [*Melrose*, 1980; *Bale et al.*, 1999; *Gopalswamy*, 2010]. As the CME-driven shocks propagate from solar corona to interplanetary space, the emission frequencies of type II radio bursts decrease with time because they are proportional to the square root of local electron densities, which fall off with heliocentric distance. The frequency (f_p) of the fundamental emission lane of a type II radio burst is directly related to the local electron density (n_e):

$$f_p = 0.009\sqrt{n_e}, \tag{1}$$

where f_p is expressed in megahertz (MHz) and n_e is in cm^{-3}. Therefore, the local electron densities can be deduced from type II radio observations.

Fast CMEs whose speeds exceed the fast-mode magnetosonic speeds can generate CME-driven shocks [*Hundhausen et al.*, 1987; *Gopalswamy et al.*, 2001, 2008]. Using the observations of SOHO/LASCO, several researchers found that the faint structures ahead of fast CMEs are the signatures of CME-driven shocks [*Ontiveros and Vourlidas*, 2009; *Vourlidas et al.*, 2013; *Lee et al.*, 2014]. By analyzing the CME-driven shock observed on 11 June 1999 from SOHO/LASCO-C2, *Bemporad and Mancuso* [2011] reported that the shock compression ratio (downstream/upstream plasma density) increases from the shock flanks to the shock center. Recently, Park et al. (manuscript in preparation, 2016) found that most of strong proton events occur when their longitudinal angular separation angles between their associated CME source regions and the magnetic footpoints of spacecraft are close to zero by examining 38 proton enhancements of 16 solar energetic particle events. Here the magnetic foot points are deduced by tracing back the magnetic field lines from the spacecraft at 1 AU to the potential field source surface at 2.5 R_s in solar corona (see section 2 of *Park et al.* [2013] for details). The above two studies indicate that the particle accelerations by CME-driven shocks should be more efficient near CME fronts than flanks. In addition to that, *Susino et al.* [2015] investigated the CME-driven shock observed on 7 June 2011 by the SOHO/LASCO coronagraphs and its associated two DH type II radio bursts by Wind/WAVES instrument [*Bougeret et al.*, 1995]. By a comparison of DH type II source regions estimated from SOHO/LASCO pB measurements with those from Wind/WAVES dynamic spectrum data based on equation (1), they showed that the DH type II radio bursts are probably generated by two different locations: one is near the front of a CME and the other is at the flank of a CME [*Susino et al.*, 2015, Figure 8].

On the other hand, several studies suggested that the source regions of DH type II radio bursts are located in the interaction regions between CME-driven shocks and streamers [*Shen et al.*, 2013; *Magdalenic et al.*, 2014]. *Shen et al.* [2013] used two well-observed DH type II radio bursts having fundamental and second harmonic emission lanes and their associated CMEs from SOHO/LASCO-C2 observations. By investigating the overlapping regions between CME-driven shock fronts and estimated DH type II source regions [*Shen et al.*, 2013, Figures 3 and 6], they found that CME shock-streamer interaction regions could be the source regions of the DH type II radio bursts. *Magdalenic et al.* [2014] examined a DH type II radio burst on 5 March 2012 by Wind/WAVES and STEREO/WAVES using a radio triangulation method [*Manning and Fainberg*, 1980; *Krupar et al.*, 2012]. They showed that the DH type II radio burst was generated by the CME shock-streamer interaction by comparing DH type II source regions from the radio triangulation method and positions of streamers [*Magdalenic et al.*, 2014, Figure 10]. In addition, there have been several reports that metric type II radio bursts are caused by the interactions between CME-driven shocks and streamers [*Mancuso and Raymond*, 2004; *Cho et al.*, 2007, 2008; *Feng et al.*, 2013; *Chen et al.*, 2014].

Several researchers have examined CEDDs by analyzing type II radio bursts and CMEs [*Robinson and Stewart*, 1985; *Reiner et al.*, 2003; *Pohjolainen et al.*, 2007]. *Robinson and Stewart* [1985] used 13 metric type II radio bursts from 1979 to 1981 with close spatial relationships between the emission heights of type II radio bursts and the heights of CME leading edges under the assumption that the lowest frequency of the second harmonic emission lane of a metric type II radio burst is generated at a CME leading edge. They estimated CEDDs by minimizing the differences between the extrapolated height-time pairs of CME leading edges and the height-time ones derived from the frequency-time pairs of type II radio bursts using assumed CEDDs [*Robinson and Stewart*, 1985, Figure 2]. They identified that the coronal electron densities of 13 events range from 3 to 7-fold *Saito* [1970] density model in the equatorial plane (hereafter Saito's model, $N_{\mathrm{Saito}}(r)$, which describes a radial CEDD in the range from about 1 to 215 R_s).

Regarding to DH type II radio bursts, *Reiner et al.* [2003] used two DH type II radio bursts, one with a metric type II radio burst and the other without. By minimizing the differences between observed frequency drift rates of DH type II radio bursts and the frequency drift rates deduced from radial speeds of CME leading edges, they found that the CEDDs are 8.2 and 5.2-fold $N_{Saito}(r)$, respectively [*Reiner et al.*, 2003, Figure 2]. *Pohjolainen et al.* [2007] obtained about 1, 7, and 5-fold $N_{Saito}(r)$, using three DH type II events by minimizing the speed differences between CME leading edges and DH type II radio bursts from different coronal density models [*Pohjolainen et al.*, 2007, Table 3]. Several examinations of individual events [*Reiner et al.*, 2005, 2007, 2008; *Bemporad and Mancuso*, 2010] using similar assumptions and methods showed that the CEDDs range from 1.2 to 2.8-fold $N_{Saito}(r)$. By using the radio triangulation method [*Manning and Fainberg*, 1980; *Krupar et al.*, 2012], *Magdalenic et al.* [2014] found that the CEDDs at the heights between about 20 and 40 R_s range from 0.4 to 2-fold $N_{Saito}(r)$. In summary, CEDDs estimated from DH type II radio bursts range from 0.4 to 8.2-fold $N_{Saito}(r)$.

The above studies have examined CEDDs using a few DH type II radio bursts. Until now, there has been no comprehensive investigation on CEDDs using DH type II radio and CME observations. In this study, we consider 399 Wind/WAVES DH type II radio bursts (from 1997 to 2012) associated with SOHO/LASCO CMEs. We select 11 limb events whose fundamental and second harmonic emission lanes are well identified. For the selected events, we determine CEDDs based on two assumptions: (1) the lowest frequency of the fundamental emission lane of a DH type II radio burst is generated at a CME leading edge; or (2) the frequency is caused by a CME shock-streamer interaction. The CEDDs of selected events are estimated by minimizing the root-mean-square error (RMSE) between the heights from CME leading edges (or CME shock-streamer interaction regions) and DH type II radio bursts. In addition, we also estimate the CEDDs of six events for both position angles (CME leading edges and the interaction regions) and the CEDD of 1 event for the position angle of the CME leading edge using pB measurements, and compare the estimated CEDDs with those from DH type II radio bursts.

This paper is organized as follows. In section 2, we describe the data selection and analysis. Result and discussion are given in section 3. A brief summary and conclusion are presented in section 4.

2. Data and Analysis

2.1. Data

We use the Wind/WAVES type II burst catalog (http://cdaw.gsfc.nasa.gov/CME_list/radio/waves_type2.html/). This catalog contains information of DH type II radio bursts detected by Wind/WAVES and their associated CMEs observed by the SOHO/LASCO as well as X-ray flares using the flare list (ftp.ngdc.noaa.gov/STP/SOLAR_DATA/SOLAR_FLARES/FLARES_XRAY/) compiled by National Geophysical Data Center (NGDC). For data selection, we take the following procedure: (1) we consider 399 events from 1997 to 2012 using the Wind/WAVES type II Burst catalog, (2) we select 160 events associated with X-ray flares whose source longitudes are greater than or equal to 60° in order to minimize projection effects using the flare list compiled by the NGDC, and (3) finally, we use 11 events that satisfy the following criteria. First, the fundamental and second harmonic emission lanes are well identified. Second, its associated CME is clearly identified in at least two frames of the LASCO-C2 or C3 field of view during the time of type II observations. The dynamic spectrum images of DH type II radio bursts are taken from the Wind/WAVES type II burst catalog. The speeds and running difference images of CMEs are taken from the SOHO/LASCO CME catalog (http://cdaw.gsfc.nasa.gov/CME_list/). For the selected events, we determine the lowest frequencies of their fundamental emission lanes and the heights of the fastest moving leading edges of their associated CMEs since we have assumed that the lowest frequencies correspond to their leading edges.

We also estimate the heights of CME shock-streamer interaction regions for nine events with satisfying the following criteria:

1. The faint structure ahead of a CME is well observed in a LASCO runninng difference image. Here the faint structure indicates the region between the CME body front and the CME shock front, which seems to be the observational signature of a CME-driven shock [*Ontiveros and Vourlidas*, 2009; *Vourlidas et al.*, 2013; *Lee et al.*, 2014];
2. A streamer or the leg of a prior CME is located near the CME;
3. The streamer deflection, which was also noted by *Sheeley et al.* [2000], occurs during the time of type II observations. Here we simply assume that the intersection points between CME leading edges and their associated streamers are the heights of type II formation.

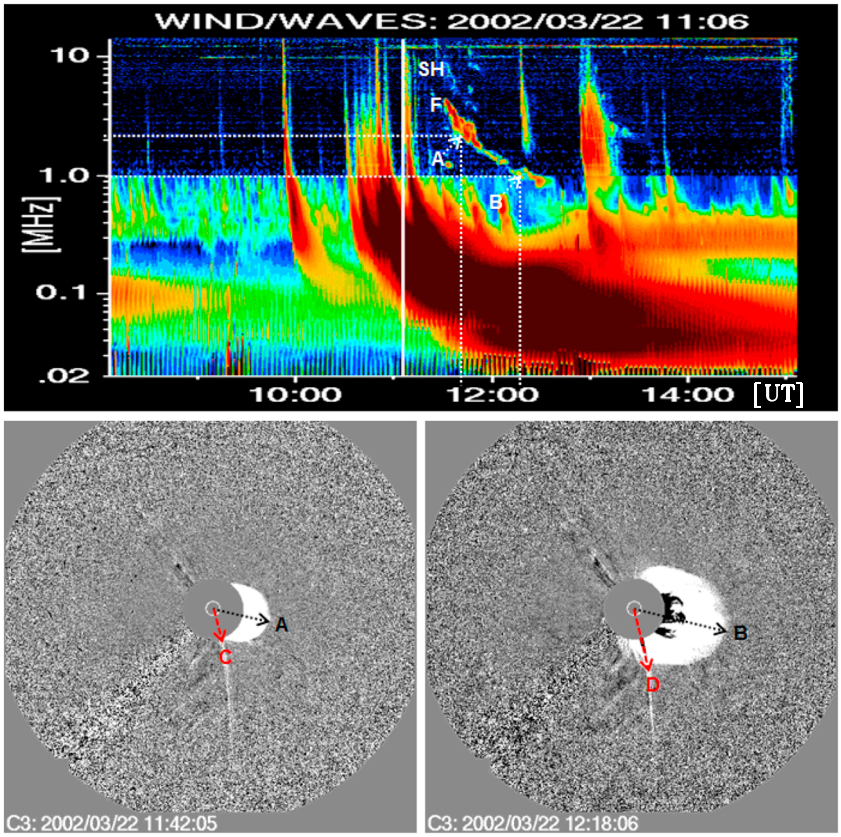

Figure 1. (top) Wind/WAVES dynamic spectrum representing one DH type II radio burst observed on 22 March 2002. Its fundamental (F) and second harmonic (SH) emission lanes are marked in the dynamic spectrum. The vertical solid line represents the first appearance time of the limb CME related to the DH type II radio burst in the LASCO-C2 field of view. The "A" and "B" indicate observed lowest frequencies of the fundamental emission lane at 11:42 UT and 12:18 UT, respectively. (Bottom) LASCO-C3 running-difference images of the limb CME observed at 11:42 UT and 12:18 UT. The directions of black and red arrows indicate the measurement position angle (MPA) corresponding to the position angle of the fastest moving front of the CME during the observations and the MPA of the streamer interacting with the CME, respectively. The A and B represent observed heights of the CME leading edges at each frame. The "C" and "D" indicate the estimated heights of CME shock-streamer interactions at each frame. The white circle represents the location and size of the solar disk.

Figure 1 shows a Wind/WAVES dynamic spectrum (top) of one DH type II radio burst on 22 March 2002 and LASCO-C3 running-difference images (bottom) of its associated limb CME. The dynamic spectrum shows its fundamental (F) and second harmonic (SH) emission lanes. The lowest frequency of the fundamental emission lane drifts from 3.4 MHz to 1 MHz between 11:30 UT and 12:18 UT. The observed lowest frequency of the fundamental emission lane and the height of the CME leading edge at 11:42 UT are 2.1 MHz and 7.84 R_s, respectively. The observed lowest frequency and the height of the CME leading edge at 12:18 UT are 1 MHz and 13.13 R_s, respectively. The estimated heights of CME shock-streamer interaction regions are 4.86 and 9 R_s at those times, respectively.

The information of 11 DH type II radio bursts and their related limb CMEs and streamers is summarized in Table 1. In columns 5–7 (9–11), the observed lowest frequency of the fundamental emission lanes of DH type II radio bursts, the height of CME leading edges (H_{CME}), and the estimated height of CME shock-streamer interaction regions (H_{C-S}) at the time of first (last) frames is presented. The measurement position angle (MPA) corresponding to the position angle of the fastest moving front of a CME during the time between the first frame and the last frame and the MPA of a streamer or the leg of a prior CME are shown in columns 13 and 15.

We cannot estimate the heights of CME shock-streamer interaction regions of 2 events (Nos. 8 and 11 in Table 1) because they do not satisfy the criteria as described above. (1) Event 8 does not have a streamer or the leg of a prior CME interacting with a CME (unsatisfied criteria 2 and 3) and (2) event 11 does not have the

Table 1. Information of 11 DH Type II Radio Bursts and Their Related Limb CMEs and Streamers[a]

	DH Type II Radio Burst	CME Appearance	First Frame				Last Frame				CME			Streamer or Prior CME Leg
Event	Date (yyyy/mm/dd)	Time (UT)	Time (UT)	f_{low} (MHz)	H_{CME} (R_s)	H_{C-S} (R_s)	Time (UT)	f_{low} (MHz)	H_{CME} (R_s)	H_{C-S} (R_s)	Source Location	MPA (deg)	V_{LASCO} (km s^{-1})	MPA (deg)
1	2000/10/16	07:27	07:27	5.8	5.46	4.28	7:42	3.2	6.78	4.58	N03W90	270	1336	360
2	2000/10/25	08:26	11:18	1.5	10.69	7.59	11:42	1.2	12.24	8.87	N09W63	250	770	20
3	2001/12/25	11:30	11:30	5.2	5.92	3.03	12:18	1.3	13.13	6.42	S28E90[b]	193	1773	60
4	2001/12/28	20:30	21:18	1.4	14.79	5.84	21:42	1.1	18.98	8.67	S26E90	162	2216	20
5	2002/03/22	11:06	11:42	2.1	7.84	4.86	12:18	1.0	13.13	9.0	S09W90	255	1750	190
6	2003/11/02	09:30	09:30	3.0	6.26	5.64	09:42	1.6	9.04	7.43	S28W90[b]	245	2036	302
7	2010/08/18	05:48	06:12	3.9	5.9	3.66	07:18	1.3	14.16	8.72	N18W88	239	1471	315
8	2011/01/13	09:36	09:36	10.3	2.99	–	09:48	7.2	3.89	–	N24E90[b]	40	664	–
9	2011/05/09	20:57	21:30	2.2	6.33	4.38	21:42	1.7	7.57	5.37	N16E88	75	1318	29
10	2011/10/21	13:25	13:25	10.9	2.93	2.5	13:36	8.6	3.29	3.27	N05W79	275	317	284
11	2012/04/15	2:24	02:36	5.5	4.2	–	2:48	3.2	6.03	–	N10E90	89	1220	115

[a]Columns 2 and 3: Starting date of a DH type II radio burst and a CME first appearance time in the LASCO-C2 field of view. Columns 4 and 8: The observing times of the first and last frames. Columns 5–7 (9–11): The lowest frequency of the fundamental emission lane of a DH type II radio burst, the height of a CME leading edge, and the height of a CME shock-streamer interaction observed at the time of the first (last) frame. Columns 12 and 14: CME source location and linear speed taken from Wind/WAVES type II Burst and SOHO/LASCO catalog. Column 13: The measurement position angle (MPA) corresponding to the position angle of the fastest moving front of a CME during the time between the first frame and the last frame. Column 15: The MPA of the streamer or the leg of a prior CME, which is interacting with a CME.

[b]Since the locational information of CME source regions in the Wind/WAVES catalog is not complete, we determined it by considering solar region summary from NOAA/SWPC and solar rotation rate with the assumption; CMEs occurred in active regions.

clear faint structures ahead of a CME in LASCO running-difference images (unsatisfied criterion 1). Therefore, it is hard to estimate their heights of type II formation.

2.2. Determination of CEDDs Using DH Type II Radio Bursts

To determine CEDDs by analyzing 11 DH type II radio bursts, we take the following procedure: (1) we assume CEDDs, which are set to scale factors multiplied by $N_{Saito}(r)$; (2) we calculate the heights of DH type II radio bursts for the observed lowest frequencies using the assumed CEDDs; and (3) finally, we select CEDDs by minimizing the RMSE between the heights from CME leading edges (or CME shock-streamer interaction regions) and the DH type II radio bursts. The RMSE is given by

$$\mathrm{RMSE}_{CME} = \sqrt{\frac{\sum_{i=1}^{n}(H_{CME} - H_{TypeII})^2}{n}}, \quad (2)$$

$$\mathrm{RMSE}_{C-S} = \sqrt{\frac{\sum_{i=1}^{n}(H_{C-S} - H_{TypeII})^2}{n}}, \quad (3)$$

where H_{CME} is the height of a CME leading edge, H_{TypeII} is the height of a DH type II radio burst, n is the number of data points for a given event, and H_{C-S} is the height of a CME shock-streamer interaction region.

Figure 2 shows examples of RMSE_{CME} and RMSE_{C-S} as a function of scale factors multiplied by $N_{Saito}(r)$ to determine CEDDs for the event shown in Figure 1 under two assumptions. DH type II bursts are generated by either (1) shocks at CME leading edges or (2) CME shock-streamer interactions. As can be seen in Figure 2 (left), the RMSE_{CME} strongly depends on the assumed CEDD, which ranges from 3.0 to 3.4-fold $N_{Saito}(r)$. The minimum RMSE_{CME} is about 0.28 R_s using 3.2-fold $N_{Saito}(r)$, which corresponds to our final estimation under the first assumption. As can be seen in Figure 2 (right), the estimated CEDD becomes 1.1-fold $N_{Saito}(r)$ with the minimum $\mathrm{RMSE}_{C-S} = 0.26\ R_s$ if we use the second assumption.

As can be seen in Figure 1, we determine the lowest frequencies of fundamental emission lanes of 11 DH type II radio bursts and the heights of their associated CME leading edges (or CME shock-streamer interaction

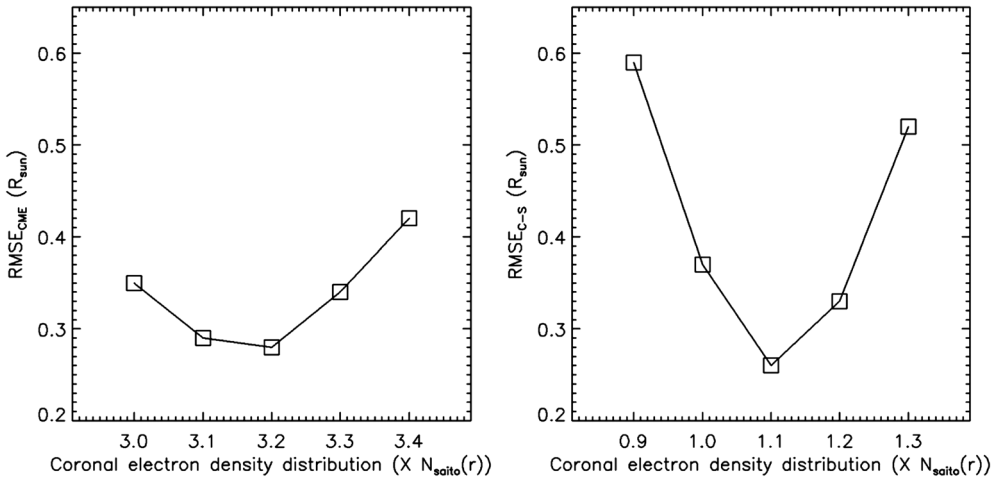

Figure 2. (left) $RMSE_{CME}$ and (right) $RMSE_{C-S}$ as a function of Saito's factor for the event shown in Figure 1. $RMSE_{CME}$ represents the height differences between CME leading edges and DH type II radio bursts from the assumed CEDD, which ranges from 3.0 to 3.4-fold $N_{Saito}(r)$. $RMSE_{C-S}$ indicates the height differences between CME shock-streamer interaction regions and DH type II radio bursts from the assumed CEDD, which ranges from 0.9 to 1.3-fold $N_{Saito}(r)$.

regions) by visual inspection of Wind/WAVES dynamic spectra and LASCO running difference images. If we consider one pixel size on dynamic spectrum images as the measurement uncertainty for the determination of the lowest frequencies, the measurement uncertainty is about 0.1 MHz at below 10 MHz and 0.3 MHz at above 10 MHz. If we consider one pixel size on LASCO running difference images as the measurement uncertainty for the determination of the heights of CME leading edges, the measurement uncertainty is about 0.04 R_s for the LASCO-C2 images and 0.16 R_s for the LASCO-C3 images. In addition, we may consider projection effects on the determination of the heights of CME leading edges since single-view coronagraphic observations are subjected to projection effects. To determine the uncertainty due to the projection effects, we use the relation between the CME propagation in the plane of the sky and that in the radial direction, which is described in Appendix A of *Leblanc et al.* [2001]. Then, the total uncertainty can be described by the root sum square of each uncertainty according to the error-propagation analysis [*Ku*, 1996].

As an example, we want to show in detail the uncertainty of a CEDD observed on 25 October 2000 (event No. 2 in Table 1). Since the source location of this limb CME is relatively closer to the Sun center than those of the other events, the uncertainty for determining the height of a CME leading edge may be higher than those of the other events. Our estimations of the uncertainty based on the above methods are given as follows. First, the measurement uncertainties for the determination of lowest frequencies and the heights of CME leading edges are about ± 0.6-fold and ± 0.2-fold $N_{Saito}(r)$, respectively. Second, the uncertainty due to the projection effects is about 0.7-fold $N_{Saito}(r)$ if we assume a half angular width of a CME is about 41°, which is an average value of halo CMEs by *Lee et al.* [2015]. The positive sign of this uncertainty is caused by the fact that the projection effects only result in the underestimation of heights. Third, the total uncertainty of the CEDD is $^{+0.9}_{-0.6}$-fold $N_{Saito}(r)$. The estimated CEDDs from DH type II radio bursts based on two assumptions and their uncertainties are presented in the columns 4 and 5 of Table 2. It should be noted that the estimated CEDDs do not mean quiescent/background CEDDs because the DH type II radio emissions are presumably originating from the locations of density enhancements at CME-driven shocks or dense streamers.

2.3. Determination of CEDDs Using pB Measurements

To estimate CEDDs using pB measurements, we use the following procedure.

1. We collect nearest pB images, which were taken from the website (http://lasco-www.nrl.navy.mil/content/retrieve/polarize/), before the first appearance times of 11 limb CMEs in the LASCO-C2 field of view.
2. We measure the CEDDs of each event along 9 angular positions around the MPA within 30° for both regions: MPAs of a CME and the streamer interacting with the CME. Here we use the data that are reasonably inverted to derive CEDDs.

Table 2. Coronal Electron Density Distributions From DH Type II Radio Bursts and pB Measurements[a]

	CME Appearance		CEDD From DH Burst	CEDD From DH Burst	pB Measurement			CEDD Around MPA	CEDD Around MPA
	Date	Time	Under Assumption 1[b]	Under Assumption 2[c]	Date	Time	LASCO	of a CME Using pB	of a Streamer Using pB
Event	(yyyy/mm/dd)	(UT)	($\times N_{Saito}(r)$)	($\times N_{Saito}(r)$)	(yyyy/mm/dd)	(UT)	FOV	($\times N_{Saito}(r)$)	($\times N_{Saito}(r)$)
1	2000/10/16	07:27	6.4 ± 0.5	2.3 ± 0.2	2000/10/15	22:55	C3	0.9 ± 0.2	1.0 ± 0.2
2	2000/10/25	08:26	$3.8 \pm^{0.9}_{0.6}$	$1.6 \pm^{0.4}_{0.3}$	2000/10/24	22:50	C3	1.1 ± 0.4	0.9 ± 0.4
3	2001/12/25	11:30	5.5 ± 0.8	0.8 ± 0.1	2001/12/24	22:50	C3	1.0 ± 0.3	1.5 ± 0.7
4	2001/12/28	20:30	8.8 ± 1.5	1.0 ± 0.2	2001/12/27	22:57	C3	1.2 ± 0.3	0.4 ± 0.2
5	2002/03/22	11:06	3.2 ± 0.6	1.1 ± 0.2	2002/03/21	22:57	C3	1.1 ± 0.4	0.9 ± 0.3
6	2003/11/02	09:30	3.2 ± 0.4	2.0 ± 0.3	2003/11/02	04:53	C3	–	–
7	2010/08/18	05:48	6.1 ± 0.9	1.7 ± 0.3	2010/08/17	22:56	C3	0.6 ± 0.2	–
8	2011/01/13	09:36	4.3 ± 0.2	–	2011/01/13	02:58	C2	–	–
9	2011/05/09	20:57	2.2 ± 0.3	0.8 ± 0.1	2011/05/08	22:56	C3	–	–
10	2011/10/21	13:25	3.6 ± 0.3	2.7 ± 0.2	2011/10/21	03:17	C2	–	–
11	2012/04/15	02:24	4.0 ± 0.2	–	2012/04/14	22:56	C3	0.6 ± 0.2	0.7 ± 0.2

[a]Columns 2 and 3: the CME first appearance date and time in the LASCO-C2 field of view. Columns 4 and 5: CEDDs estimated from a DH type II radio burst under the first and second assumptions. The uncertainties of the estimated CEDDs from DH type II radio bursts are also presented. Columns 6–8: the pB measurement date, time, and LASCO field of view. Columns 9 and 10: CEDDs around MPAs of a CME and the streamer interacting with the CME using pB measurements. The deviations between the average values of the estimated CEDDs and their upper (or lower) value are also presented.

[b]DH type II radio bursts are generated by shocks at CME leading edges.

[c]DH type II radio bursts are generated by CME shock-streamer interactions.

3. The CEDDs obtained from pB measurements are converted into the form of scale factors multiplied by $N_{Saito}(r)$ by minimizing the differences between the electron densities from pB measurements and assumed CEDDs [*Gopalswamy and Yahiro*, 2011].

As a result, we are able to reasonably estimate the CEDDs of six events (No. 1, 2, 3, 4, 5, and 11 in Tables 1 and 2) for both MPAs and the CEDD of event No. 7 for MPA of the CME using pB measurements in the LASCO-C3 field of view. Figure 3 shows an example of coronal electron densities around MPA of the CME, which was shown in Figure 1, as a function of heliocentric distance. We find that the estimated CEDDs range from 0.7 to 1.4-fold $N_{Saito}(r)$. The average value of the CEDDs is about 1.1-fold $N_{Saito}(r)$. We also find that the average of CEDDs around MPA of the streamer is about 0.9-fold $N_{Saito}(r)$. The estimated CEDDs around both MPAs using pB measurements are shown in the columns 9 and 10 of Table 2. We cannot estimate the CEDDs of four events (No. 6, 8, 9, and 10 in Tables 1 and 2) for both MPAs and the CEDD of event No. 7 for MPA of the streamer region, because their pB data were not successfully inverted into the radial profiles of CEDDs by using the Solar Software routine "pb_inverter.pro."

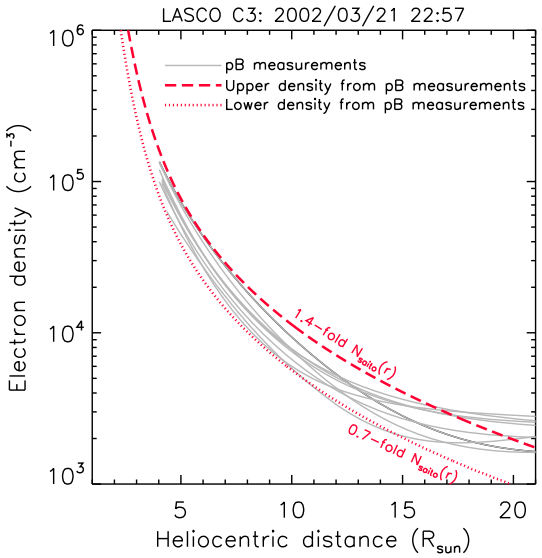

Figure 3. Coronal electron densities as a function of heliocentric distance. The solid lines indicate the CEDDs of the event, which was shown in Figure 1, around MPA of the CME using pB measurements in the LASCO-C3 field of view. The red long dashed and dotted lines represent upper and lower CEDDs obtained from pB measurements, respectively.

The estimated CEDDs might have uncertainties because the inversion method simply assumes that an CEDD is spherically symmetric geometry [*van de Hulst*, 1950]. Regarding to this, several researchers examined the validation of pB measurements by comparing coronal electron densities from pB measurements of coronagraphs with those from the other methods such as density sensitive line measurements of UV

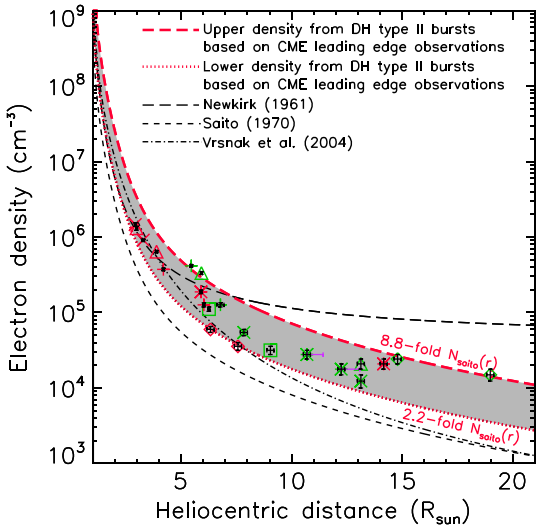

Figure 4. Scatterplot between the coronal electron densities of 11 events and the heights of their associated CME leading edges. The green plus, asterisk, triangle, diamond, cross, and square symbols indicate the electron densities of events No. 1, 2, 3, 4, 5, and 6, respectively. The red asterisk, triangle, diamond, cross, and plus symbols represent the electron densities of events No. 7, 8, 9, 10, and 11, respectively. The red long dashed and dotted lines show upper and lower CEDDs estimated from 11 DH type II radio bursts under the first assumption: DH type II radio bursts are generated by shocks at CME leading edges. The black long dashed, dashed, and dash-dotted lines indicate CEDDs corresponding to *Newkirk* [1961], *Saito* [1970], and *Vrsnak et al.* [2004] models. The black vertical and horizontal error bars indicate the measurement uncertainties for the determination of lowest frequencies and the heights of CME leading edges, respectively. The purple horizontal error bars show the uncertainties due to the projection effects.

spectroscopy and a tomography reconstruction [*Gibson et al.*, 1999; *Lee et al.*, 2008; *Wang and Davila*, 2014]. They found that coronal electron densities using pB measurements from about 1.5 to 4 R_s are similar to those from other methods within a factor of 2. The estimated CEDDs using pB measurements at large solar distances, like LASCO-C3 data, might have uncertainties caused by polarized contributions of the F corona because the polarized contributions beyond 5 R_s cannot be negligible [*Koutchmy and Lamy*, 1985; *Mann*, 1992]. To minimize this uncertainty, we determine scale factors of $N_{\mathrm{Saito}}(r)$ using the pB measurements below 5 R_s. Another possible uncertainty of pB measurements in the LASCO-C3 field of view is caused by the quantum efficiency and wavelength of the LASCO-C3 flight CCD, which is estimated to be about 10% [*Morrill et al.*, 2006].

3. Result and Discussion

3.1. CEDDs From DH Type II Bursts Based on CME Leading Edge Observations

Figure 4 shows coronal electron densities of 11 events at the heights of leading edges of their associated CMEs (various symbols), as well as their CEDDs (shadow areas). We find that the estimated CEDDs at the heights between about 3 and 20 R_s range from 2.2 to 8.8-fold $N_{\mathrm{Saito}}(r)$, which becomes 1.9 to 10.3-fold if their uncertainties are included (Table 2). Our estimated CEDDs are similar to those (3 ~ 7-fold $N_{\mathrm{Saito}}(r)$) from the previous analysis using metric type II radio bursts and CMEs [*Robinson and Stewart*, 1985], while our estimation in the lower range is a slightly higher than those (0.4 ~ 8.2-fold $N_{\mathrm{Saito}}(r)$) from the previous studies using DH type II radio bursts [*Reiner et al.*, 2003, 2005; *Pohjolainen et al.*, 2007; *Reiner et al.*, 2007, 2008; *Bemporad and Mancuso*, 2010]. We note that there were three events whose CEDDs are near 1-fold $N_{\mathrm{Saito}}(r)$ in the previous studies [*Reiner et al.*, 2005; *Pohjolainen et al.*, 2007; *Magdalenic et al.*, 2014]. Two events were estimated from the data with low frequency range below 1 MHz [*Reiner et al.*, 2005; *Magdalenic et al.*, 2014], which does not satisfy our data selection criteria; in fact, it is hard to determine the lowest frequencies of DH type II emission lanes below 1 MHz, because the emission frequencies of DH type II radio bursts are usually mixed with the emission frequencies of other type II and type III radio bursts as shown in Figure 1 (top). The remaining one was obtained from the analysis of a halo CME having projection effects [*Pohjolainen et al.*, 2007]. If this effect is taken into account, the estimated CEDD becomes a higher fold of $N_{\mathrm{Saito}}(r)$.

We compare coronal electron densities between our results and the previous density models: *Newkirk* [1961], *Saito* [1970], and *Vrsnak et al.* [2004] models, which have been widely used for analyzing type II radio bursts [*Vrsnak et al.*, 2004; *Cho et al.*, 2005, 2008; *Pohjolainen et al.*, 2013; *Subramanian and Shanmugaraju*, 2013]. We find that the coronal electron densities from our results are similar to Newkirk's model and the hybrid model of *Vrsnak et al.* [2004] in solar corona from about 3 to 5 R_s. The average of estimated coronal densities at the heights between about 3 and 20 R_s is about 5-fold $N_{\mathrm{Saito}}(r)$ with the standard deviation (SD) of 1.8-fold. This result is similar to that of *Robinson and Stewart* [1985] who suggested that the preferred CEDD for metric type II radio bursts is 5-fold $N_{\mathrm{Saito}}(r)$.

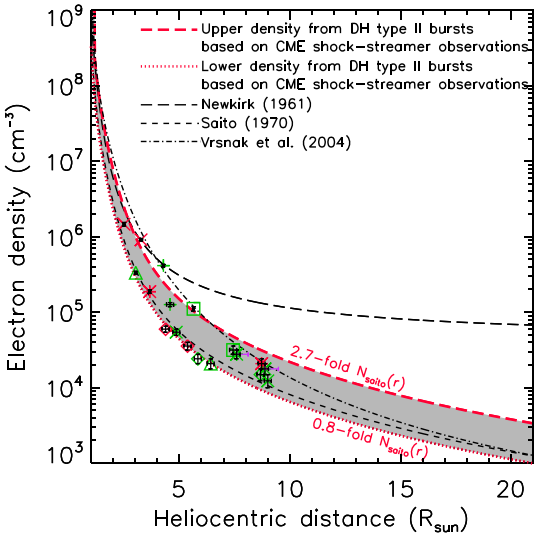

Figure 5. Scatterplot between the coronal electron densities of nine events and the heights of their associated CME shock-streamer interaction regions. The green plus, asterisk, triangle, diamond, cross, and square symbols indicate the electron densities of events No. 1, 2, 3, 4, 5, and 6 respectively. The red asterisk, diamond, and cross symbols represent the electron densities of events No. 7, 9, and 10, respectively. The red long dashed and dotted lines show upper and lower CEDDs estimated from nine DH type II radio bursts under the second assumption; DH type II radio bursts are generated by CME shock-streamer interactions. The black lines and error bars are same as in Figure 4.

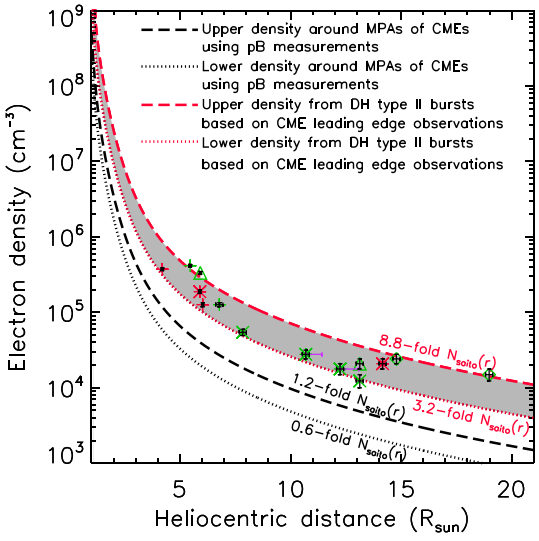

Figure 6. Comparison of the CEDDs of seven events (No. 1, 2, 3, 4, 5, 7, and 11 in Tables 1 and 2) around MPAs of CMEs using pB measurements with those (shadow areas) from their associated DH type II radio bursts under the first assumption. The black long dashed and dotted lines indicate upper and lower CEDDs obtained from pB measurements, respectively. The red long dashed and dotted lines represent upper and lower CEDDs estimated from the DH type II radio bursts, respectively. The symbols and error bars are the same as in Figure 4.

3.2. CEDDs From DH Type II Bursts Based on CME Shock-Streamer Observations

Figure 5 shows coronal electron densities of nine events at the heights of their associated CME shock-streamer interaction regions (various symbols), as well as their CEDDs (shadow areas). We find that the estimated CEDDs at the heights between about 3 and 10 R_s range from 0.8 to 2.7-fold $N_{Saito}(r)$, which becomes 0.7 to 2.9-fold if their uncertainties are included (Table 2). Our estimated CEDDs are much lower than those (3 ~ 7-fold $N_{Saito}(r)$) from the previous analysis using metric type II radio bursts [*Robinson and Stewart*, 1985]. The CEDDs are similar to those (1 ~ 3-fold $N_{Saito}(r)$) from the previous studies using DH type II radio bursts [*Reiner et al.*, 2005; *Pohjolainen et al.*, 2007; *Reiner et al.*, 2007, 2008; *Bemporad and Mancuso*, 2010], while they are much lower than those (5.2 ~ 8.2-fold $N_{Saito}(r)$) from the results using DH type II data with and without metric type II radio bursts [*Reiner et al.*, 2003; *Pohjolainen et al.*, 2007]. We note that our coronal electron density range is similar to that (0.4~2-fold $N_{Saito}(r)$) from the radio triangulation method [*Magdalenic et al.*, 2014].

We compare coronal electron densities between our results and the previous density models. We find that most of the coronal electron densities from our results are similar to Saito's model in solar corona from about 3 to 7 R_s except for a few events whose electron densities are similar to the hybrid model of *Vrsnak et al.* [2004]. The average of estimated coronal densities at the heights between 3 and 10 R_s is 1.5-fold $N_{Saito}(r)$ with SD of 0.6-fold, which is similar to that of *Magdalenic et al.* [2014].

3.3. CEDDs From pB Measurements

We also estimate the CEDDs of seven events using pB measurements of SOHO/LASCO. As seen in the columns 9 and 10 of Table 2, the estimated CEDDs around both MPAs of CMEs and streamers range from 0.4 to 1.5-fold $N_{Saito}(r)$. These values are consistent with those (0.4 ~ 1.6-fold $N_{Saito}(r)$) from the previous measurements [*Reiner et al.*, 2003; *Gopalswamy and Yahiro*, 2011; *Feng et al.*, 2013]. In addition, our scale factors are similar to those (0.4 ~ 2-fold $N_{Saito}(r)$) from *Magdalenic et al.* [2014] who used radio imaging data from the radio triangulation method to examine coronal electron densities at the heights between about 20 and 40 R_s. Our results together with the previous ones show

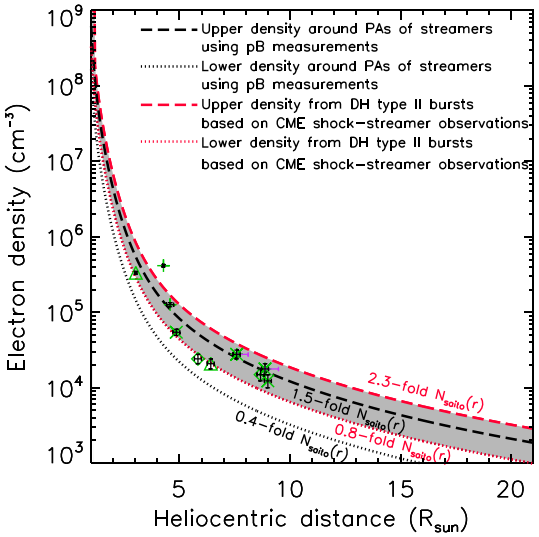

Figure 7. Comparison of CEDDs of five events (No. 1, 2, 3, 4, and 5 in Tables 1 and 2) around MPAs of streamer regions using pB measurements with those (shadow areas) from their associated DH type II radio bursts under the second assumption. The black long dashed and dotted lines indicate upper and lower CEDDs obtained from pB measurements, respectively. The red long dashed and dotted lines represent upper and lower CEDDs estimated from the DH type II radio bursts, respectively. The symbols and error bars are the same as in Figure 5.

that the CEDD from about 3 to 40 R_s can be reasonably approximated by 1-fold $N_{Saito}(r)$.

3.4. Comparison of CEDDs

Figure 6 shows a comparison of the CEDDs of seven events for MPAs of CMEs using pB measurements with those from their associated DH type II radio bursts under the first assumption. We find that the average of CEDDs obtained from pB measurements is about 1-fold $N_{Saito}(r)$ with SD of 0.2-fold. This result is significantly smaller than that (about 5-fold $N_{Saito}(r)$ with SD of 1.8-fold) from the DH type II radio bursts based on the CME leading edge observations.

Figure 7 shows a comparison of the CEDDs of five events for MPAs of streamer regions using pB measurements with those from their associated DH type II radio bursts under the second assumption. We find that the average of CEDDs obtained from pB measurements is about 1-fold $N_{Saito}(r)$ with SD of 0.3-fold. This result is well consistent with that (about 1-fold $N_{Saito}(r)$ with SD of 0.5-fold) from the DH type II radio bursts based on the CME shock-streamer interactions.

Recently, several researchers have studied the source locations of DH type II radio bursts by analyzing a comprehensive data set: Wind/WAVES dynamic spectra, SOHO/LASCO CMEs, and pB measurements [*Shen et al.*, 2013; *Susino et al.*, 2015]. Using two well-observed DH type II radio bursts having fundamental and second harmonic emission lanes, and their associated CMEs from SOHO/LASCO-C2 observations, *Shen et al.* [2013] examined the overlapping regions between CME-driven shock fronts and estimated DH type II source regions. As a result they found that CME shock-streamer interaction regions could be source regions of the DH type II radio bursts [*Shen et al.*, 2013, Figures 3 and 6]. In a similar way, *Susino et al.* [2015] showed that one DH type II radio burst may be generated near the flank of a CME interacting with a nearby streamer [*Susino et al.*, 2015, Figure 8]. In addition, early theoretical researchers suggested that quasi-perpendicular shocks, which occur at CME shock-streamer interaction regions, can be more likely to accelerate electrons by the shock drift acceleration mechanism [*Holman and Pesses*, 1983; *Wu*, 1984]. Our results together with the above studies have shown that CME shock-streamer interactions could be a plausible origin for generating DH type II radio bursts.

The DH type II radio bursts might be produced by shock-electron accelerations in the CME flank regions without streamers. To examine this possibility, we compare the CEDDs of 5 events (No. 1, 2, 3, 4, and 5 in Tables 1 and 2) from DH type II bursts based on the observations of CME flank regions, which were taken from regions without CME shock-streamer interactions, with those obtained from pB measurements. Under this assumption, the average of estimated CEDDs from 5 to 15 R_s is about 3-fold $N_{Saito}(r)$ with SD of 1.5-fold. The average of CEDDs obtained from pB measurements is about 1-fold $N_{Saito}(r)$ with SD of 0.1-fold, which is significantly smaller than that (about 3-fold $N_{Saito}(r)$ with SD of 1.5) from DH type II bursts based on the CME flanks without CME shock-streamer interactions. This result suggests that CME flank regions without CME shock-streamer interactions are not preferable for generating DH type II radio bursts.

4. Summary and Conclusion

In this study, we have determined CEDDs by analyzing DH type II radio observations based on two assumptions; DH type II bursts are generated by either (1) shocks at CME leading edges or (2) CME shock-streamer interactions. For this, we consider 399 Wind/WAVES DH type II radio bursts (from 1997 to 2012) associated with SOHO/LASCO CMEs. We select a special data set (11 events) satisfying the following criteria: (1) the source longitude of a CME is greater than or equal to 60°; (2) the fundamental and second harmonic

emission lanes are well identified; and (3) its associated CME is clearly identified in at least two frames of the LASCO-C2 or C3 field of view during the time of type II observations. The CEDDs of selected events are estimated by minimizing the RMSE between the heights from CME leading edges (or CME shock-streamer interaction regions) and DH type II bursts. In addition, we also estimate CEDDs of six events for both MPAs (CME leading edges and the interaction regions) and the CEDD of one event for MPA of the CME leading edge using pB measurements.

The main results of this study can be summarized as follows. First, under the first assumption, the average of estimated CEDDs of 11 events at the heights between about 3 and 20 R_s is about 5-fold $N_{\mathrm{Saito}}(r)$ with SD of 1.8-fold. Second, under the second assumption, the average of estimated CEDDs of nine events at the heights between 3 and 10 R_s is 1.5-fold $N_{\mathrm{Saito}}(r)$ with SD of 0.6-fold. Third, while the CEDDs of seven events using pB measurements are significantly smaller than those based on the first assumption, the CEDDs of five events using pB measurements are well consistent with those based on the second assumption. Our main findings are also consistent with the recent other observations as follows. First, the CEDD with about 1-fold $N_{\mathrm{Saito}}(r)$ is supported by the radio triangulation method [*Magdalenic et al.*, 2014]. Second, the CME shock-streamer interaction regions as the locations of DH type II bursts are supported by the radio triangulation method [*Magdalenic et al.*, 2014] as well as the analysis of CME, type II, and pB measurements [*Shen et al.*, 2013; *Susino et al.*, 2015]. Our results together with those from recent observations show that not only about 1-fold $N_{\mathrm{Saito}}(r)$ is a proper CEDD for analyzing DH type II bursts but also CME shock-streamer interactions could be a plausible origin for generating DH type II radio bursts.

Acknowledgments

Thanks to the two reviewers for their constructive comments and helpful suggestions on an earlier version of the manuscript. This work was supported by the BK21 plus program through the National Research Foundation (NRF) funded by the Ministry of Education of Korea, the National Radio Research Agency/Korean Space Weather Center, Basic Science Research Program through the NRF funded by the Ministry of Education (NRF-2013R1A1A2012763, 2013R1A1A2058409) and NRF of Korea grant funded by the Korean Government (NRF-2013M1A3A3A02042232). The Wind/WAVES type II Burst catalog is generated and maintained at the CDAW Data Center by NASA. The Wind/WAVES instrument was designed and built as a joint effort of the Paris-Meudon Observatory, the University of Minnesota, and the Goddard Space Flight Center. The CME catalog is generated and maintained at the CDAW Data Center by NASA and The Catholic University of America in cooperation with the Naval Research Laboratory. The SOHO/LASCO data used here are produced by a consortium of the Naval Research Laboratory (USA), Max-Planck-Institut fuer Aeronomie (Germany), Laboratoire d'Astronomie (France), and the University of Birmingham (UK). SOHO is a project of international cooperation between the ESA and NASA. Wind/WAVES data were obtained from Wind/WAVES type II burst catalog (http://cdaw.gsfc.nasa.gov/CME_list/radio/waves_type2.html/). X-ray flares were taken from the flare list compiled by NGDC (ftp.ngdc.noaa.gov/STP/SOLAR_DATA/SOLAR_FLARES/FLARES_XRAY/). SOHO/LASCO CME data were obtained from SOHO/LASCO CME catalog (http://cdaw.gsfc.nasa.gov/CME_list/). SOHO/LASCO pB data were taken from from the website (http://lasco-www.nrl.navy.mil/content/retrieve/polarize/).

References

Akmal, A., J. C. Raymond, A. Vourlidas, B. Thompson, A. Ciaravella, Y.-K. Ko, M. Uzzo, and R. Wu (2001), SOHO observations of a coronal mass ejection, *Astrophys. J.*, *553*(6), 922–934, doi:10.1086/320971.

Alvarez, H., and F. T. Haddock (1973), Solar wind density model from km-wave type III bursts, *Sol. Phys.*, *29*(3), 197–209, doi:10.1007/BF00153449.

Aschwanden, M. J. (2005), *Physics of the Solar Corona: An Introduction With Problems and Solutions*, 1st ed., Springer-Praxis Books in Astron. and Planet. Sci., Chichester, U. K.

Bale, S. D., M. J. Reiner, J.-L. Bougeret, M. L. Kaiser, S. Krucker, D. E. Larson, and R. P. Lin (1999), The source region of an interplanetary type II radio burst, *Geophys. Res. Lett.*, *26*(6), 1573–1576, doi:10.1029/1999GL900293.

Bemporad, A., and S. Mancuso (2010), First complete determination of plasma physical parameters across a coronal mass ejection-driven Shock, *Astrophys. J.*, *720*(9), 130–143, doi:10.1088/0004-637X/720/1/130.

Bemporad, A., and S. Mancuso (2011), Identification of super- and subcritical regions in shocks driven by coronal mass ejections, *Astrophys. J.*, *739*(2), L64, doi:10.1088/2041-8205/739/2/L64.

Bougeret, J.-L., et al. (1995), Waves: The radio and plasma wave investigation on the Wind spacecraft, *Space Sci. Rev.*, *71*(2), 231–263, doi:10.1007/BF00751331.

Brueckner, G. E., et al. (1995), The Large Angle Spectroscopic Coronagraph (LASCO), *Sol. Phys.*, *162*(12), 357–402, doi:10.1007/BF00733434.

Chen, Y., G. Du, L. Feng, S. Feng, K. Xiangliang, F. Guo, B. Wang, and G. Li (2014), A solar type II radio burst from coronal mass ejection-coronal ray interaction: Simulatneous radio and extreame ultraviolet imaging, *Astrophys. J.*, *787*(1), 59, doi:10.1088/0004-637X/787/1/59.

Cho, K.-S., Y.-J. Moon, M. Dryer, A. Shanmugaraju, C. D. Fry, Y.-H. Kim, S.-C. Bong, and Y.-D. Park (2005), Examination of type II origin with SOHO/LASCO observations, *J. Geophys. Res.*, *110*, A12101, doi:10.1029/2004JA010744.

Cho, K.-S., J. Lee, Y.-J. Moon, M. Dryer, S.-C. Bong, Y.-H. Kim, and Y.-D. Park (2007), A study of CME and type II shock kinematics based on coronal density measurement, *Astron. Astrophys.*, *461*(1), 1121–1125, doi:10.1051/0004-6361:20064920.

Cho, K.-S., S.-C. Bong, Y.-H. Kim, Y.-J. Moon, M. Dryer, A. Shanmugaraju, J. Lee, and Y.-D. Park (2008), Low coronal observations of metric type II associated CMEs by MLSO coronameters, *Astron. Astrophys.*, *491*(12), 873–882, doi:10.1051/0004-6361:20079013.

Fainberg, J., and R. G. Stone (1971), Type III solar radio burst storms observed at low frequencies. III: Streamer density, inhomogeneities, and solar wind speed, *Sol. Phys.*, *17*(4), 392–401, doi:10.1007/BF00150042.

Feng, S. W., Y. Chen, X. L. Kong, G. Li, H. Q. Song, X. S. Feng, and F. Guo (2013), Diagnostics on the source properties of a type II radio burst with spectral bumps, *Astrophys. J.*, *767*(1), 29, doi:10.1088/0004-637X/767/1/29.

Gibson, S. E., A. Fludra, F. Bagenal, D. Biesecker, G. del Zanna, and B. Bromage (1999), Solar minimum streamer densities and temperatures using whole sun month coordinated data sets, *J. Geophys. Res.*, *104*(5), 9691–9700, doi:10.1029/98JA02681.

Gopalswamy, N. (2010), Corona mass ejections: A summary of recent results, Proceedings of the 20th Slovak National Solar Physics Workshop, edited by I. Dorotovic, Slovak Central Observatory, pp. 108–130.

Gopalswamy, N., and S. Yahiro (2011), The strength and radial profile of the coronal magnetic field from the standoff distance of a coronal mass ejection-driven shock, *Astrophys. J. Lett.*, *736*(1), L17, doi:10.1088/2041-8205/736/1/L17.

Gopalswamy, N., A. Lara, M. L. Kaiser, and J.-L. Bougeret (2001), Near-Sun and near-Earth manifestations of solar eruptions, *J. Geophys. Res.*, *106*(11), 25,261–25,278, doi:10.1029/2000JA004025.

Gopalswamy, N., S. Yashiro, H. Xie, S. Akiyama, E. Aguilar-Rodriguez, M. L. Kaiser, R. A. Howard, and J.-L. Bougeret (2008), Radio-quiet fast and wide coronal mass ejections, *Astrophys. J.*, *674*(2), 560–569, doi:10.1086/524765.

Hayes, A. P., A. Vourlidas, and R. A. Howard (2001), Deriving the electron density of the solar corona from the inversion of total brightness measurements, *Astrophys. J.*, *548*(2), 1081–1086, doi:10.1086/319029.

Holman, G. D., and M. E. Pesses (1983), Solar type II radio emission and the shock drift acceleration of electrons, *Astrophys. J.*, *267*, 837–843, doi:10.1086/160918.

Howard, R. A., et al. (2008), Sun Earth Connection Coronal and Heliospheric Investigation (SECCHI), *Space Sci. Rev.*, *136*(1–4), 67–115, doi:10.1007/s11214-008-9341-4.

Hundhausen, A. J., T. E. Holzer, and B. C. Low (1987), Do slow shocks precede some coronal mass ejections?, *J. Geophys. Res.*, *92*(10), 11,173–11,178, doi:10.1029/JA092iA10p11173.
Keenan, F. P., P. Brekke, P. B. Byrne, and C. J. Greer (1995), The OV 1371.29A/1218.35A emission-line ratio in solar and stellar spectra, *Mon. Not. R. Astron. Soc.*, *276*(10), 915–922.
Ko, Y.-K., J. C. Raymond, T. H. Zurbuchen, P. Riley, J. M. Raines, and L. Strachan (2006), Abundance variation at the vicinity of an active region and the coronal origin of the slow solar wind, *Astrophys. J.*, *646*(8), 1275–1287, doi:10.1086/505021.
Koutchmy, S., and P. L. Lamy (1985), The F-corona and the circum-solar dust evidences and properties, in *Properties and Interactions of Interplanetary Dust*, pp. 63–74, Springer, Netherlands.
Krupar, V., O. Santolik, B. Cecconi, M. Maksimovic, X. Bonnin, M. Panchenko, and A. Zaslavsky (2012), The Goniopolarimetric inversion using SVD: An application to type III radio bursts observed by STEREO, *J. Geophys. Res.*, *117*, A06101, doi:10.1029/2011JA017333.
Ku, H. H. (1996), Notes on the use of propagation of error formulas, *J. Res. Natl. Bureau Standards*, *70C*(10), 263–273.
Leblanc, Y., G. A. Dulk, and J.-L. Bougeret (1998), Tracing the electron density from the corona to 1 AU, *Sol. Phys.*, *183*(11), 165–180, doi:10.1023/A:1005049730506.
Leblanc, Y., G. A. Dulk, A. Vourlidas, and J.-L. Bougeret (2001), Tracing shock waves from the corona to 1 AU: Type II radio emission and relationship with CMEs, *J. Geophys. Res.*, *106*(11), 25,301–25,312, doi:10.1029/2000JA000260.
Lee, H., Y.-J. Moon, H. Na, S. Jang, and J.-O. Lee (2015), Are 3-D coronal mass ejection parameters from sing-view observations consistent with multi-view ones?, *J. Geophys. Res. Space Physics*, *120*, 10,237–10,249, doi:10.1002/2015JA021118.
Lee, J.-O., Y.-J. Moon, J.-Y. Lee, K.-S. Lee, S. Kim, and K. Lee (2014), Are the faint structures ahead of solar coronal mass ejections real signatures of driven shocks?, *Astrophys. J. Lett.*, *796*(1), L16, doi:10.1088/2041-8205/796/1/L16.
Lee, J.-Y., J. C. Raymond, Y.-K. Ko, and K.-S. Kim (2009), Three-dimensional structure and energy balance of a coronal mass ejection, *Astrophys. J.*, *692*(2), 1271–1286, doi:10.1088/0004-637X/692/2/1271.
Lee, K.-S., Y.-J. Moon, K.-S. Kim, J.-Y. Lee, K.-S. Cho, and G. S. Choe (2008), Comparison of SOHO UVCS and MLSO MK4 coronameter densities, *Astron. Astrophys.*, *486*(8), 1009–1013, doi:10.1051/0004-6361:20078976.
Magdalenic, J., C. Marque, V. Krupar, M. Mierla, A. N. Zhukov, L. Rodriguez, M. Maksimovic, and B. Cecconi (2014), Tracking the CME-driven shock wave on 2012 March 5 and radio triangulation of associated radio emission, *Astrophys. J.*, *791*(2), 115, doi:10.1088/0004-637X/791/2/115.
Mancuso, S., and J. C. Raymond (2004), Coronal transients and metric type II radio bursts. I. Effects of geometry, *Astron. Astrophys.*, *413*(1), 363–371, doi:10.1051/0004-6361:20031510.
Mann, I. (1992), The solar F-corona—Calculations of the optical and infrared brightness of circumsolar dust, *Astron. Astrophys.*, *261*(7), 329–335.
Manning, R., and J. Fainberg (1980), A new method of measuring radio source parameters of a partially polarized distributed source from spacecraft observations, *Space Sci. Instrum.*, *5*, 161–181.
Melrose, D. B. (1980), The emission mechanisms for solar radio bursts, *Space Sci. Rev.*, *26*(5), 3–38, doi:10.1007/BF00212597.
Morrill, J. S., C. M. Korendyke, G. E. Brueckner, F. Giovane, R. A. Howard, M. Koomen, D. Moses, S. P. Plunkett, and A. Vourlidas (2006), Calibration of the SOHO/LASCO C3 white light coronagraph, *Sol. Phys.*, *233*(2), 331–372, doi:10.1007/s11207-006-2058-1.
Newkirk, G., Jr. (1961), The solar corona in active regions and the thermal origin of the slowly varying component of solar radio radiation, *Astrophys. J.*, *133*(5), 983–1013, doi:10.1086/147104.
Noci, G., J. L. Kohl, and G. L. Withbroe (1987), Solar wind diagnostics from Doppler-enhanced scattering, *Astrophys. J.*, *315*(4), 706–715, doi:10.1086/165172.
Ontiveros, V., and A. Vourlidas (2009), Quantitative measurements of coronal mass ejection-driven shocks from LASCO observations, *Astrophys. J.*, *693*(3), 267–275, doi:10.1088/0004-637X/693/1/267.
Parenti, S., B. J. I. Bromage, G. Poletto, G. Noci, J. C. Raymond, and G. E. Bromage (2000), Characteristics of solar coronal streamers. Element abundance, temperature and density from coordinated CDS and UVCS SOHO observations, *Astron. Astrophys.*, *363*(11), 800–814.
Park, J., D. E. Innes, R. Bucik, and Y.-J. Moon (2013), The source regions of solar energetic particles detected by widely separated spacecraft, *Astrophys. J.*, *779*(2), 184, doi:10.1088/0004-637X/779/2/184.
Pinfield, D. J., M. Mathioudakis, F. P. Keenan, K. J. H. Phillips, and W. Curdt (1998), The O V 1213.9 Angstroms forbidden line in the quiet Sun, *Astron. Astrophys.*, *340*(12), L15–17.
Pohjolainen, S., L. van Driel-Gesztelyi, J. L. Culhane, P. K. Manoharan, and H. A. Elliott (2007), CME propagation characteristics from radio observations, *Sol. Phys.*, *224*(8), 167–188, doi:10.1007/s11207-007-9006-6.
Pohjolainen, S., H. Allawi, and E. Valtonen (2013), Origin of wide-band IP type II bursts, *Astron. Astrophys.*, *558*, A7, doi:10.1051/0004-6361/201220688.
Reiner, M. J., A. Vourlidas, O. C. St. Cyr, J. T. Burkepile, R. A. Howard, M. L. Kaiser, N. P. Prestage, and J.-L. Bougeret (2003), Constraints on coronal mass ejection dynamics from simultaneous radio and white-light observations, *Astrophys. J.*, *590*(6), 533–546, doi:10.1086/374917.
Reiner, M. J., B. V. Jackson, D. F. Webb, D. R. Mizuno, M. L. Kaiser, and J.-L. Bougeret (2005), Coronal mass ejection kinematics deduced from white light (Solar Mass Ejection Imager) and radio (Wind/WAVES) observations, *J. Geophys. Res.*, *110*, A09S14, doi:10.1029/2004JA010943.
Reiner, M. J., S. Krucker, D. E. Gary, B. L. Dougherty, M. L. Kaiser, and J.-L. Bougeret (2007), Radio and white-light coronal signatures associated with the RHESSI Hard X-Ray event of 2002 July 23, *Astrophys. J.*, *657*(3), 1107–1116, doi:10.1086/510827.
Reiner, M. J., K.-L. Klein, M. Karlicky, K. Jiricka, A. Klassen, M. L. Kaiser, and J.-L. Bougeret (2008), Solar origin of the radio attributes of a complex type III burst observed on 11 April 2001, *Sol. Phys.*, *249*(6), 337–354, doi:10.1007/s11207-008-9189-5.
Robinson, R. D., and R. T. Stewart (1985), A positional comparison between coronal mass ejection events and solar type II bursts, *Sol. Phys.*, *97*(5), 145–157, doi:10.1007/BF00152984.
Saito, K. (1970), A non-spherical axisymmetric model of the solar K corona of the minimum type, *Ann. Tokyo Astron. Obs. Ser.*, *2*(12), 53–120.
Saito, K., A. J. Poland, and R. H. Munro (1977), A study of the background corona near solar minimum, *Sol. Phys.*, *55*(11), 121–134, doi:10.1007/BF00150879.
Sheeley, N. R., W. N. Hakala, and Y.-M. Wang (2000), Detection of coronal mass ejection associated shock waves in the outer corona, *J. Geophys. Res.*, *105*(3), 5081–5092, doi:10.1029/1999JA000338.
Shen, C., C. Liao, Y. Wnag, P. Ye, and S. Wang (2013), Source region of the decameter-hectometric type II radio burst: Shock-streamer interaction region, *Sol. Phys.*, *282*(2), 543–552, doi:10.1007/s11207-012-0161-z.
Subramanian, S. P., and A. Shanmugaraju (2013), Study of interacting CMEs and DH type II radio bursts, *Astrophys. Space Sci.*, *344*(4), 305–312, doi:10.1007/s10509-012-1347-4.
Susino, R., A. Bemporad, and S. Mancuso (2015), Physical conditions of coronal plasma at the transit of a shock driven by a coronal mass ejection, *Astrophys. J.*, *812*(2), 119, doi:10.1088/0004-637X/812/2/119.

Uzzo, M., L. Strachan, A. Vourlidas, Y.-K. Ko, and J. C. Raymond (2006), Physical properties of a 2003 April quiescent streamer, *Astrophys. J.*, *645*(7), 720–731, doi:10.1086/504286.

Wang, T., and J. M. Davila (2014), Validation of spherically symmetric inversion by use of a tomographically reconstructed three-dimensional electron density of the solar corona, *Sol. Phys.*, *289*(10), 3723–3745, doi:10.1007/s11207-014-0556-0.

Wu, C. S. (1984), A fast Fermi process—Energetic electrons accelerated by a nearly perpendicular bow shock, *J. Geophys. Res.*, *89*, 8857–8862, doi:10.1029/JA089iA10p08857.

van de Hulst, H. C. (1950), The electron density of the solar corona, *Bull. Astron. Inst. Netherlands*, *11*, 135.

Vourlidas, A., B. J. Lynch, R. A. Howard, and Y. Li (2013), How many CMEs have flux ropes? Deciphering the signatures of shocks, flux ropes, and prominences in coronagraph observations of CMEs, *Sol. Phys.*, *284*(5), 179–201, doi:10.1007/s11207-012-0084-8.

Vrsnak, B., J. Magdalenic, and P. Zlobec (2004), Band-splitting of coronal and interplanetary type II bursts. III. Physical conditions in the upper corona and interplanetary space, *Astron. Astrophys.*, *413*(1), 753–763, doi:10.1051/0004-6361:20034060.